

A Reminder of its Brittleness: Language Reward Shaping May Hinder Learning for Instruction Following Agents

Sukai Huang, Nir Lipovetzky and Trevor Cohn*

School of Computing and Information Systems, The University of Melbourne, Australia
sukaih@student.unimelb.edu.au, {nir.lipovetzky, trevor.cohn}@unimelb.edu.au

Abstract

Teaching agents to follow complex written instructions has been an important yet elusive goal. One technique for enhancing learning efficiency is language reward shaping (LRS). Within a reinforcement learning (RL) framework, LRS involves training a reward function that rewards behaviours precisely aligned with given language instructions. We argue that the apparent success of LRS is brittle, and prior positive findings can be attributed to weak RL baselines. Specifically, we identified suboptimal LRS designs that reward partially matched trajectories, and we characterised a novel reward perturbation to capture this issue using the concept of loosening task constraints. We provided theoretical and empirical evidence that agents trained using LRS rewards converge more slowly compared to pure RL agents. Our work highlights the brittleness of existing LRS methods, which has been overlooked in the previous studies.¹

1 Introduction

In recent years, large-scale language models have shown exceptional performance in downstream tasks (Fei et al. 2022; Bommasani et al. 2021; Duan et al. 2022; Alayrac et al. 2022), leading to increased interests in integrating these pretrained language models with task-specific control policies for instruction following agents (Luketina et al. 2019). Previous literature on instruction following often proposed end-to-end models that directly mapped language instructions and state observations to task-specific low-level control. However, this tight coupling with the task environment prevented the use of general pretrained models.

To address this limitation, attempts have been made to develop instruction following agents featuring separate reasoning and policy models, allowing pretrained models to be seamlessly integrated. One such methodology is Language Reward Shaping (LRS), which leverages pretrained multi-modal or unimodal models to formulate reward functions rewarding RL agents’ behaviors in accordance with expert instructions. (see Figure 1). From the perspective of RL researchers, LRS offers a means of tackling the sparse reward challenge by introducing supplementary reward signals through language information.

*Now at Google DeepMind

¹Code and replication materials is released at Github https://github.com/sino-huang/brittleness_of_lrs.

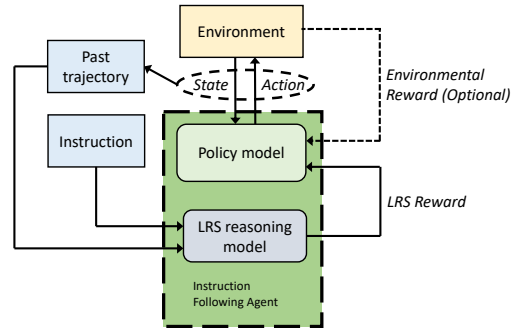


Figure 1: A Language Reward Shaping framework

The core mechanism of LRS involves compressing high-dimensional semantic vectors of natural language instructions encoded by pretrained large models into scalar rewards. However, despite its apparent simplicity, we have observed that agents trained with LRS rewards often exhibit slower convergence compared to purely RL-trained agents in practical scenarios. Thus, the key research question that we aim to answer in this paper is: *what causes the deterioration of LRS methods?*

Our contributions in this paper are summarised as follows: 1) we identify suboptimal LRS architecture designs that reward partially matched trajectories (see Figure 2); 2) we introduce a novel form of reward perturbation that characterizes this issue through the concept of relaxing task constraints; 3) we offer both theoretical and empirical evidence demonstrating that, compared to a reinforcement learning algorithm that effectively explores the state-space, LRS can underperform due to its tendency to reward partially matched trajectories. However, it is important to clarify that we don’t seek to undermine the value of LRS methodology. Rather, our goal is to offer a perspective on potential factors contributing to slow convergence.

2 Related Work

Language Reward Shaping (LRS) is a term formally defined by Goyal, Niekum, and Mooney (2019, 2021). It involves constructing a reward function that rewards agent behaviours aligned with expert instructions. The technique has been implemented across various domains, ranging from di-

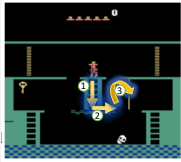
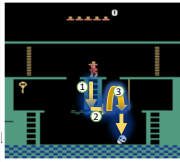

Instruction: Climb down the ladder and then jump to the top of the yellow rope		
trajectory τ_1 Reward: 1.0 (perfect)	trajectory τ_2 Reward: 0.5	trajectory τ_3 Reward: 0.5
		
The agent followed the instruction perfectly.	The agent performed the required action sequence but since it did not know the effect of the conveyor belt, it did not jump at the right position and ended up falling off.	The agent completed the subgoals but in the wrong order. It jumped to the yellow rope first and then climbed up & down the ladder.

Figure 2: In practice, partially matched trajectories can still be assigned rewards that are reduced but not entirely void.

ologue systems (Ouyang et al. 2022), visual language navigation (Wang et al. 2019) to recommender systems (Lin et al. 2022). While prior studies on LRS (Kaplan, Sauer, and Sosa 2017; Ibarz et al. 2018; Wang et al. 2019; Du et al. 2023) have touted its efficacy, they have not discussed the potential collapse of the system due to rewarding partially matched trajectories.

Reward Perturbation Analysis is an orthogonal work that studies the influence of reward perturbation on the performance of RL algorithms. Previous research on reward perturbation has focused on relatively limited types of poisoned rewards, such as reversing the sign of the numeric rewards (Zhang et al. 2021; Ilahi et al. 2021), adaptive reward attack (Huang et al. 2017; Zhang et al. 2020), reward delay attack (Sarkar et al. 2022), and action-triggered reward manipulation (Wang et al. 2021). In comparison, our research introduces and evaluates the effects of a new variant of reward perturbation, rooted in the concept of relaxing task constraints, which is implicitly inherent in existing LRS methods.

3 Problem Setup

3.1 Sparse Reward MDP Environment

In this work, we define our task as a MDP tuple $\langle S, A, T, s_0, S_G, S_L, R^{env} \rangle$. Here, S is the finite set of states, A is the finite set of actions, and $T : S \times A \rightarrow S$ is a deterministic state transition function where, for any state $s \in S$ and action $a \in A$, the next state s' is given by $T(s, a)$. The process starts at the unique initial state s_0 . S_G is a set of goal states, and S_L is a set of terminating states in which every action causes a deterministic transition back to itself with zero reward. The sparse environmental reward function is given by $R^{env} : S \times A \times S \rightarrow \mathbb{R}$, where for any s, a, s' :

$$R^{env}(s, a, s') = \begin{cases} r & \text{if } s' \text{ in } S_G \\ 0 & \text{otherwise} \end{cases}$$

where r is a positive constant representing the reward for reaching a goal state.

In addition, we adopted the subsequent assumption:

Assumption 3.1 (Deterministic Policies). We assume deterministic policies $\pi : S \rightarrow A$, which map each state to a specific action.

Corollary 3.2 (Bijective Correspondence). Due to the deterministic nature of the transition function T and policies π , there exists a bijective correspondence between a policy π and its trajectory τ^π . A trajectory τ^π from start state s_0 to a terminating state is a sequence of states and actions $(s_0, a_0, s_1, a_1, \dots)$ such that $s_{i+1} = T(s_i, a_i)$ where $a_i = \pi(s_i)$.

Adhering to the problem formulation presented by Abel et al. (2021), we further define:

- *Policy Universe*, Π : The set of all possible policies for the MDP.
- *Acceptable Policies*, Π_G : A subset of Π such that any policy $\pi \in \Pi_G$ has its trajectory τ^π terminating in a goal state $s_g \in S_G$. Formally, $\Pi_G = \{\pi \in \Pi \mid \exists s_g \in S_G : s_g \text{ is reachable from } s_0 \text{ under } \pi\}$

This configuration leads to the following proposition:

Proposition 3.3 (Abel et al. (2021)). The sparse environmental reward function R^{env} can effectively distinguish policies from Π_G against the complete policy universe Π , but cannot make distinctions of preference within Π_G .

3.2 Formulation of Expert Instructions

Drawing on the principle that expert instructions capture preferences for a subset of acceptable policies, we model the alignment of a trajectory to an expert instruction as a constraint matching problem. In this framework, we conceptualize the instruction as a composite of action, state, and temporal constraints:

Definition 3.4 (Constraint Composition). Let’s consider expert instructions that reflect preferences for a subset of acceptable policies, denoted by $\Pi_{INST} \subseteq \Pi_G$. In this context, we defined that:

1. An *action constraint*, denoted by C_a , is derived from the action observed in the preferred trajectories taken by acceptable policies. Formally, $C_a := \{a \mid a \in \tau^\pi, \pi \in \Pi_{INST} \subseteq \Pi_G, a \in A\}$.
2. A *state constraint*, denote by C_s , is based on states traversed in the preferred trajectories of acceptable policies. Formally, $C_s := \{s \mid s \in \tau^\pi, \pi \in \Pi_{INST} \subseteq \Pi_G, s \in S\}$.
3. A *temporal constraints*, C_t , captures the sequential relationship among transitions $T(s_i, a_i)$ in a trajectory. There exists a myriad of formal languages that can express temporal relationships (e.g., Linear Temporal Logic (LTL) (Camacho et al. 2019)). More detailed information is in Appendix E.

Based on the definition provided above, a trajectory aligns with an expert instruction if and only if it satisfies the associated action, state, and temporal constraints. If the trajectory meets only some of the constraints, we term it as being “partially matched” with the instruction.

The choice of formulation has its roots in the compositional nature of natural language. Research indicates that leveraging the compositionality of language enhances

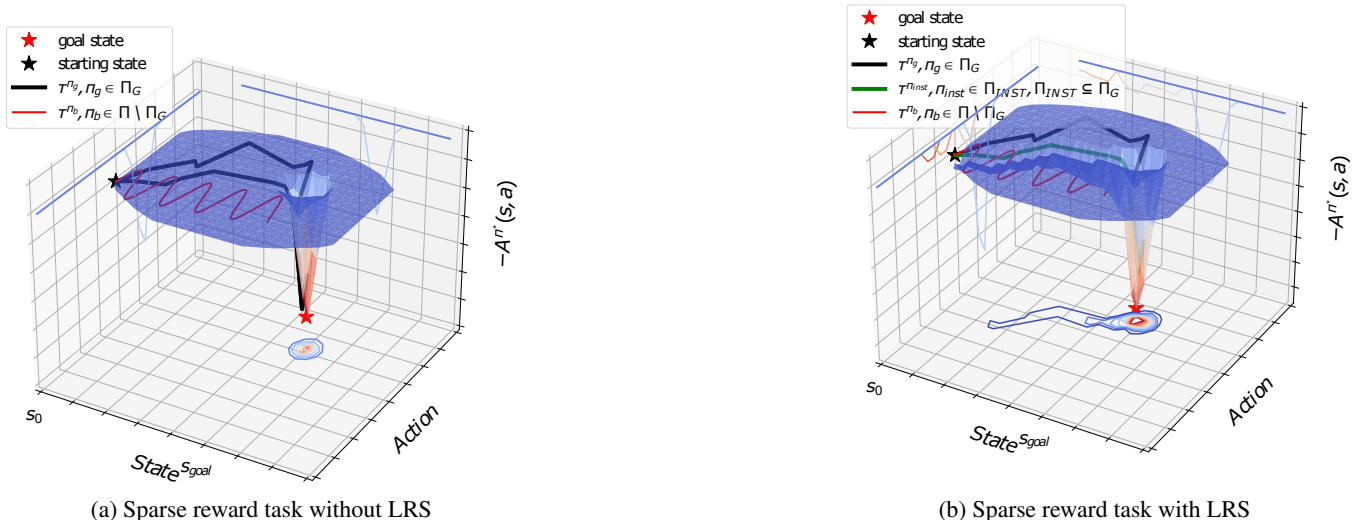


Figure 3: A schematic drawing of how LRS helps RL algorithms by providing a gradient on the value function manifold towards the goal state. In a sparse reward environment, finding an acceptable policy $\pi_g \in \Pi_G$ relies heavily on the exploration ability of the agent. In contrast, LRS provides auxiliary rewards to set Π_{INST} , creating a gradient towards the goal state.

problem-solving capacities in language models (Akyürek and Andreas 2022; Bhambri, Kim, and Choi 2023; Drexler, Seipp, and Geffner 2021; Liu, Palacios, and Muise 2022). By situating our instruction-following problem within a constraint satisfaction context, we push for a more structured interpretation of language instructions, aligning with insights from Yang et al. (2021).

3.3 Shaping Reward Function by Instructions

Language Reward Shaping aims to provide reward signals for RL agents when their trajectories match expert preferences encoded in natural language instructions, as depicted in Figure 3. Mathematically, LRS constructs a potential-based shaping reward function F to provide immediate auxiliary rewards for RL algorithms, with convergence guaranteed in theory.

Proposition 3.5 (Convergence guarantee). *A reward shaping function that gives rewards when agent’s trajectory matches the language instruction can be written in the form*

$$F_t = F(s_t, a_t, s_{t-1}, a_{t-1}) = \Phi(s_t, a_t) - \gamma^{-1} \Phi(s_{t-1}, a_{t-1})$$

where a_t is the action for the current state s_t at time t ; $\Phi : S \times A \rightarrow \mathbb{R}$ is a real-valued function. Then, the optimal policy $\pi^* \in \Pi_G$ in the original task environment setting will remain optimal in the new setting where the reward signal at time t becomes $R_t^{env} + F_t$

While the shaping reward function, as described in Equation 1, appears *non-Markovian* due to its reliance on how past behavior aligns with the instruction, it’s pivotal to understand that the policy’s training remains unaffected provided it is an on-policy model. A detailed explanation of this behavior and its implications can be found in Appendix D. We say that this form of reward function is potential-based (Ng, Harada, and Russell 1999; Wiewiora, Cottrell, and

Elkan 2003). While theoretical indications suggest that a potential-based LRS function can enhance the learning efficiency of RL algorithms, our investigation unveils that practical convergence can be notably hindered by the issue of rewarding partially matched trajectories.

4 The Brittleness of LRS

In this section, we will particularly focus on the specific concern of rewarding partially matched trajectories and provide theoretical evidence demonstrating its impact on the convergence rate of RL algorithms. To illustrate this, we will use Actor Critic as an example.

4.1 Suboptimal Compression of the Information – the Bottleneck in LRS Models

LRS operates by compressing high-dimensional semantic vectors into scalar reward signals. However, this compression introduces ambiguity and imprecision about what should be rewarded.

One crucial aspect contributing to the limitation of LRS architecture is the *smoothness of the model*. As illustrated in Figure 4, LRS models predominantly employ gradient-based learning methods. Among prevalent LRS implementations, two primary prediction styles emerge for matching instruction-trajectory pairs: cosine similarity and binary classification. Works by Kaplan, Sauer, and Sosa (2017); Kant et al. (2022); Du et al. (2023) have harnessed cosine similarity in their output layers. In contrast, binary classification output layers are used in works like Goyal, Niekum, and Mooney (2019) and Wang et al. (2019). The inherent characteristic of gradient-based learning to allocate non-zero rewards, even for imperfect input alignments, is a double-edged sword. While it leads to a smoother and more exploratory learning process, it concurrently increases the likelihood of agents exploiting towards suboptimal paths. It gets

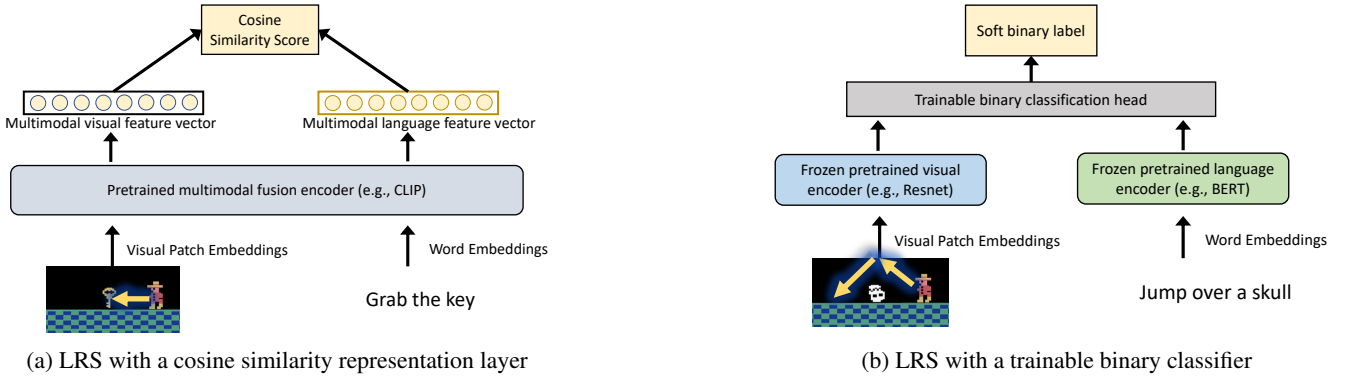


Figure 4: An illustration of two suboptimal design classes in Language Reward Shaping models. Both design classes fail to avoid rewarding partially matched trajectories.

more challenging when attempting to reinforce specific behaviors within a trajectory that were intended to be pivotal in achieving a particular reward.

Another challenge is the *handling of temporal information*. Both the game environment and the language instructions involve temporal aspects, but Transformer models (Vaswani et al. 2017), which are commonly used as the backbone architecture in LRS models, may not adequately capture chronological ordering (Pham et al. 2020). While Transformer models can learn temporal dependencies to some extent, there is little in the pre-training to enforce this strictly. Thus, the reward function can be less sensitive to the ordering of action execution. Additionally, the temporal dimension collapses when compressing instructions into scalars. These aforementioned challenges ultimately contribute to the concrete issue of *rewarding partially matched trajectories*.

4.2 Rewarding Partially Matched Trajectories

Rewarding partially matched trajectories leads to challenges for learning agents in distinguishing between preferred and non-preferred behavior segments. As shown in the examples in Figure 2, these false positive rewards might misguide LRS agents into thinking they’re on the right track, leading to the repetition of suboptimal behaviors.

Adding to this complexity is the *compositionality of natural language*. While a finer partitioning of the training dataset may aid in distinguishing between matched and unmatched pairs, an atomic sentence that cannot be further broken down at the natural language level can still encompass multiple constraints. For instance, the atomic sentence “cut down the tree” contains both the action constraint “cutting down” and the object constraint “tree”. Thus, even with meticulous annotation, assigning a clear-cut binary label (0 or 1) to instruction and trajectory pairs is not straightforward. It is due to the possibility of trajectories partially aligning with an atomic instruction, thereby blurring the distinction between a complete match and a mismatch. Therefore, in practice, it is infeasible to establish a uniform threshold for distinguishing whether a reward reduction is due to a hard negative or the estimation error.

4.3 Reduction of Convergence Rate

Convergence rate refers to the number of training iterations needed to learn an ϵ -optimal policy. However, the exact convergence rate calculations for RL algorithms provided in prior research (Agarwal et al. 2021; Xiao 2022) cannot be directly applied in this context. This limitation arises from their reliance on the assumption that the initial state is sampled from a certain distribution. Therefore, an alternative way of analysing the convergence rate is to measure the probability of picking acceptable policies (i.e., $P(\pi \in \Pi_G)$) over each update iteration.

Theorem 4.1 (Convergence rate reduction). *In Actor-Critic algorithm, gradient ascent on $Q(s, a)\pi_{\theta_i}(a|s)$ pushes the next updated policy $\pi_{\theta_{i+1}}$ in the direction provided by the Q value function. In the presence of false positive rewards, the gradient of $Q(s, a)\pi(a|s)$ can be expressed as follows:*

$$\begin{aligned} \nabla_{\theta} Q_{\phi}(s, a)\pi_{\theta}(a|s) &= \text{const} \cdot \mathbb{E}[G^{\pi \in \Pi_L}] \nabla_{\theta} \pi_{\theta}(a|s) \\ &+ (\mathbb{E}[G^{\pi \in \Pi_G}] - \mathbb{E}[G^{\pi \in \Pi_L}]) P(\pi \in \Pi_G) \nabla_{\theta} \pi_{\theta}(a|s) \end{aligned}$$

where Π_G is the set of acceptable policies; Π_L is an arbitrary set of suboptimal policies that are partially consistent; G^{π} is the cumulative rewards by executing policy π in one episode.

The proof is in Appendix D.2. Since the goal of the learning agent is to maximise $P(\pi \in \Pi_G)$ (i.e., to converge to an acceptable policy), we can see that the second term provides the target direction with rate $(\mathbb{E}[G^{\pi \in \Pi_G}] - \mathbb{E}[G^{\pi \in \Pi_L}])$. Therefore, the ascent rate will decrease when the expectation of the rollout cumulative false positive rewards gets higher. Moreover, the first term $\text{const} \cdot \mathbb{E}[G^{\pi \in \Pi_L}] \nabla_{\theta} \pi_{\theta}(a|s)$ can be regarded as the deviation of target direction. It shows that the level of deviation is also positively proportional to the magnitude of expectation of the rollout cumulative false positive rewards. Therefore, rewarding partially matched trajectories is shown to reduce the convergence rate of the RL algorithm. Note that in this setting, rewards for partially matched trajectories are of a lower magnitude (i.e., $\mathbb{E}[G^{\pi \in \Pi_G}] > \mathbb{E}[G^{\pi \in \Pi_L}]$). Consequently, LRS models can theoretically converge, despite the existence of false positive rewards. However, our empirical evaluation revealed

Table 1: Reward rules for the simulated LRS model: Rule 1 rewards only fully matched trajectories, while Rule 2 allows partial matches with reduced reward magnitude; Rule 3 further relax the temporal ordering constraints and allows for rewards to be obtained out of order.

Name	Rewarding Set	Magnitude
Rule 1: Fully Matched	$\{\tau^{\pi_{inst}} \mid \pi_{inst} \in \Pi_{C_a} \cap \Pi_{C_s} \cap \Pi_{C_t}\}$	$r = 1.0$
Rule 2: Partially Matched	$\{\tau^{\pi_{inst}} \mid \pi_{inst} \in \Pi_{C_a} \cup \Pi_{C_s} \cap \Pi_{C_t}\}$	$r = 0.5$ if π_{inst} is partially matched
Rule 3: Relaxed Ordering	$\{\tau^{\pi_{inst}} \mid \pi_{inst} \in \Pi_{C_a} \cup \Pi_{C_s}\}$	$r = 1.0$ if π_{inst} is fully matched

that agents trained with LRS rewards exhibit slower convergence rates compared to pure RL agents.

5 Experiments and Result Analysis

5.1 Experimental Setup

We conduct experiments in the Atari game Montezuma’s Revenge, a challenging benchmark with sparse rewards, to evaluate the impact of rewarding partially matched trajectories on LRS agents. We conduct our experiments in three distinct rooms (A1, A2, and B3) to test the consistency of our analysis across different tasks. We collected top-rated instruction sentences from game forums relating to these levels. Our RL policy model is based on PPO and RND RL algorithm (Burda et al. 2018). Specifically, RND algorithm gives auxiliary rewards when agents reach unseen states, which is a widely accepted curiosity-driven exploration strategy. We use Area Under the Learning Curve (AUC) metric. This AUC metric, having been previously endorsed in studies like Goyal, Niekum, and Mooney (2019), emerges as a more fitting indicator of the convergence rate for RL models. For more details of AUC, refer to Appendix A.

Non-Simulated LRS Model While earlier models cited in Section 2 were often tailored to domain-specific tasks and limited by the technologies of their time, they all operate within a similar LRS framework. Given this commonality, we felt it justified to construct our own model, enabling us to sidestep those domain and technological constraints. Our non-sim LRS model incorporates state-of-the-art sentence embedding models and visual encoders. Preliminary evaluations revealed that existing open-sourced pre-trained multimodal models (e.g., BLIP (Li et al. 2023) and mPLUG (Xu et al. 2023)) had a poor performance in encoding cartoon images. Addressing this, our LRS model implemented a trainable binary classification output layer, as depicted in Figure 4b. Specifically, the model uses a T5 sentence transformer (Raffel et al. 2020) as the language encoder; a masked auto-encoding pre-training objective (Seo et al. 2022); soft-discretisation with YOLOv7 (Wang, Bochkovskiy, and Liao 2022) for the visual observation encoder; and GATED XATTN module (Alayrac et al. 2022) as the binary classifier backbone. The fine-tuning involved 5000 annotated Montezuma’s Revenge clips from Amazon Mechanical Turk, supplemented by contrastive learning using hard negatives. Ablation studies and more de-

tails can be found in Appendix G. It is important to clarify that the issue of rewarding partially matched trajectories is not confined to particular choices of LRS encoders. Instead, it arose from scalar compression and smooth gradient-based learning, as discussed in Section 4.

Simulated LRS Model In our efforts to assess the impact of rewarding partially matched trajectories without the interference of other factors such as domain shift, poor data quality, and approximation error due to the choice of multimodal architectures, we devised a simulated LRS model. The model compares the sequence of past actions and states of the agent with predefined target trajectory sets that map to each instruction sentence. It subsequently assigns rewards in the following modes (see Table 1):

- Rule 1 dispenses rewards exclusively for chronologically arranged trajectories that align perfectly with each instruction sentence.
- Rule 2 allows for partial trajectory matches but with diminished reward magnitude, while preserving the temporal order.
- Rule 3 further removes the temporal ordering constraints and permits rewards even if obtained out of sequence.

Our careful design ensures that the simulated LRS model already represents the upper bound, making it a valuable tool to demonstrate the issue caused by rewarding partially matched trajectories. Further implementation details are in Appendix B.

5.2 Main Results

Results are reported in Table 2. Several important observations can be made:

1. LRS techniques have shown enhanced performance compared to weak RL baselines like PPO. While agents trained solely with PPO struggled to navigate through all three rooms, incorporating LRS into PPO (i.e., PPO+LRS) did find solutions, albeit with modest success rates. However, the non-simulated LRS agent remained challenged by room A2, a task that necessitates intricate sequential decision-making.

2. In our qualitative assessment of the Room A2 task, both non-simulated and simulated LRS agents displayed instances of receiving false positive rewards, as depicted in Figure 2. These misleading rewards prompted the LRS agents to persistently adopt suboptimal strategies, hindering them from completing the desired long trajectories. Ad-

Table 2: Performance of agents in Montezuma’s Revenge game, measured by AUC (higher is better), as well as success rate for perturbed rewards tolerance. Baseline denoted as B. \star indicates statistical significance ($p < 0.05$).

Model	AUC	SR
PPO (Schulman et al. 2017)	all failed	0%
PPO+RND (B) (Burda et al. 2018)	0.550±0.066	100%
PPO + Sim LRS Rule 1	0.287±0.048	100%
PPO+RND + Non-Sim LRS	0.069±0.139 \star	16.7%
PPO+RND + Sim LRS Rule 1	0.608±0.073	100%
PPO+RND + Sim LRS Rule 2	0.183±0.187 \star	73.3%
PPO+RND + Sim LRS Rule 3	0.051±0.116 \star	16.7%

ditionally, the movement heatmaps in Figures 5b and 5c showed a noticeable similarity, indicating that the simulated LRS model (Rule 2) accurately captured the behavior of the real LRS model. The use of the simulated LRS model thus provided a valuable means of highlighting practical issues with LRS implementations.

3. The AUC value of both non-simulated and simulated LRS agents (Rule 2 and Rule 3) underperformed versus pure PPO+RND agents. This deterioration of learning efficiency is statistically significant. Both non-simulated and simulated agents were unable to reach a goal state in certain training runs. In particular, the success rate of non-simulated LRS agents experienced a notable drop, indicating the destabilizing effect of false positive rewards on the learning process.

4. The algorithm completely failed to converge when LRS models neglected the temporal ordering (i.e., Rule 3). The heatmap in Figure 5d showed that the learning agent kept pursuing rewards from the last instruction sentence (i.e., “walk left to the door”). However, the agent did not escape the room by simply executing the last instruction because a key was required to unlock the door. It suggests that the agent tends to be trapped by local minima that are close to the initial state s_0 when temporal ordering is disregarded.

5.3 Analysis of Instructions of Varied Granularity

As part of the test, we also examined how different levels of granularity affect performance. We simulated a less detailed instruction in following two ways: 1) skipping intermediate steps and 2) neglecting an entire aspect of information, such as omitting actions details. The two types of less detailed instructions are illustrated in Table 3. Communicating with a low granularity of information is very common as human communicators often believe that some intermediate steps are not important or they intentionally omit common-sense information under the assumption that they share the same context with their audience (Mitkov 2014).

Our result showed that the two types of less detailed instructions led to different performance outcomes. As shown in Figure 6, we observed no statistically significant deterioration in learning efficiency when intermediate steps are skipped. This suggested that RL algorithms are capable of interpolating missing information based on the given context and therefore can quickly recover from the missing interme-

diated steps. However, when removing a whole dimension of constraints, finding the goal would take more training time with a larger variance. This indicated that in such instances, the model essentially relearns from scratch and thereby lacking any prior commonsense knowledge to extrapolate the missing dimension of the information.

5.4 Effectiveness of Language Reward Shaping

Our results also revealed that agents with an ideal language reward shaping model might still learn more slowly than a vanilla PPO+RND RL agent in difficult environments. We attribute this observation to the fact that LRS agents are constrained to follow instructions that may not cover all the acceptable policies (i.e., $\Pi_{INST} \subset \Pi_G$). Therefore, the trade-off between a smoother value function manifold and the reduced size of the goal policy set can result in slower learning, as a large number of acceptable policies are pruned out. For instance, the heatmap in Figure 5a showed that PPO+RND agent found an alternative solution path (i.e., directly jumping from the cliff) rather than the one suggested by the instruction (i.e., climbing down the ladder). Nevertheless, we speculate that LRS can have a positive effect when $|\Pi_{INST}| \approx |\Pi_G|$. This would require building an LRS model that can interpret more general language information, such as manuals and strategies, to cover almost all possible circumstances and solutions. This suggests the need for a more intelligent language model that can ground general information to agent actions.

6 Conclusion

The combination of a powerful foundation language backbone, such as T5 (Raffel et al. 2020), with state-of-the-art RL algorithms might be seen as a solution to effectively tackle sequential decision-making problems. However, our study highlights the need for a careful design of the knowledge transfer mechanism from large pretrained models to domain-specific models to achieve effective results. Specifically, we observed that 1) the challenges of LRS models when compressing high-dimensional vectors into scalars are not contingent upon specific language models or the quality of the training dataset; 2) LRS models that reward partially matched trajectories are statistically slower than pure RL

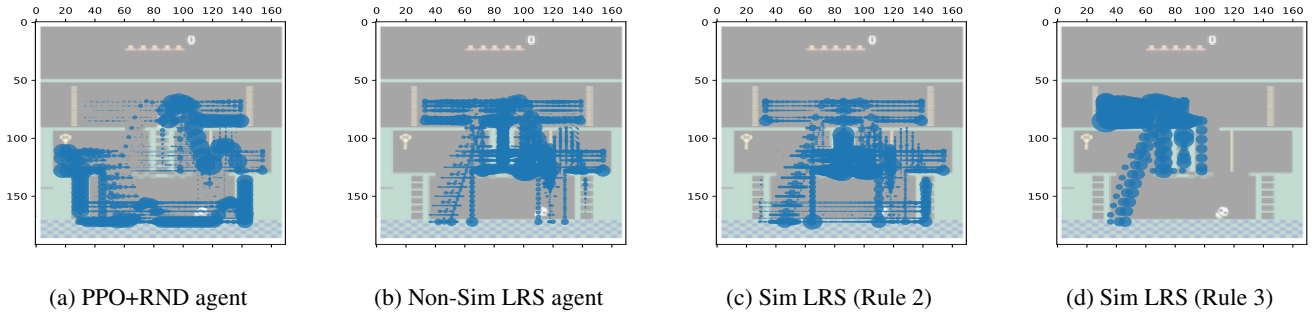


Figure 5: Movement heatmap for agents in different settings

Table 3: Less detailed instructions represented in trajectory sequences, with human readable examples.

Type	Representation	Example
1	$(s_0, a_n, s_n, \dots, a_{kn}, s_{kn}), n, k \in \mathbb{Z}^+$	Climb down the ladder and walk right on the conveyor belt , after that, jump to the yellow rope.
2	$(s_0, s_1, s_2, \dots, s_k), k \in \mathbb{Z}^+$	Climb down To the ladder and walk right on to the conveyor belt, after that, jump to the yellow rope.

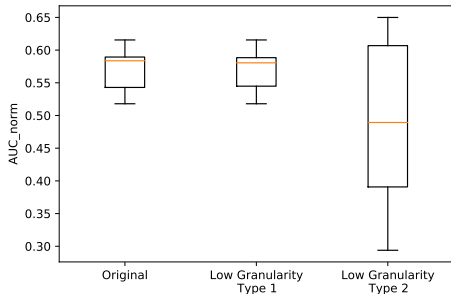


Figure 6: Comparison of the learning efficiency across different granularity – Type 1 skips intermediate steps; Type 2 neglects a whole dimension.

agents in the Montezuma sparse reward environment. Furthermore, the introduction of reward perturbation by loosening task constraints presents a novel extension to the existing types of poisoned rewards and also highlights the unique challenges involved in using LRS. We stress that our goal is not to dismiss the concept of using language instructions to provide auxiliary rewards for training agents. Instead, we aim to shed light on the severe bottleneck faced by existing LRS approaches and the need for addressing these fundamental limitations. By recognizing and addressing these challenges, we can pave the way for more effective and robust LRS architectures in the future.

While we believe that LRS models which perform poorly in Montezuma would face even more significant convergence issues in more complex real-world scenarios, we acknowledge the limited scope of this work – the impact of rewarding partially matched trajectories may vary depend-

ing on the tasks’ difficulty levels. For instance, in the case of Montezuma room A1, which is a simpler task compared to room A2 and B3, we observed that LRS agents learned faster compared to PPO+RND agents. Nevertheless, the results from the simulated LRS models indicated that the convergence was still severely hampered by the presence of false positive rewards. Specifically, we observed that the influence of false positive rewards may be alleviated in environments with smaller action spaces, as demonstrated by Du et al. (2023). Moreover, we recognise that the benefits of suboptimal LRS can outweigh its drawbacks in scenarios where exploration is undesirable. For instance, 1) in dangerous real-world environments, exploration can be costly; or 2) in tasks that require repeated actions, naive exploration may not provide additional benefits.

We suggest two directions for improvement. First is to consider the compositionality of the language instructions. One potential approach is to turn the scalar reward signals into vectorised multi-label rewards. This could mitigate ambiguity in reward signals by explicitly representing the level of satisfaction for different types of constraints. Second, the type of rewarding shall not be limited to immediate numerical rewards for RL algorithms. We could formulate the learning problem as a trajectory optimisation problem (e.g., Janner et al. (2022)), using language instructions to directly upvote a set of matched trajectories. This may help to avoid cumulative rollout errors caused by single-step reward models, and thereby improving the learning efficiency.

References

Abel, D.; Dabney, W.; Harutyunyan, A.; Ho, M. K.; Littman, M.; Precup, D.; and Singh, S. 2021. On the expressivity of markov reward. *Advances in Neural Information Processing Systems*, 34: 7799–7812.

- Agarwal, A.; Kakade, S. M.; Lee, J. D.; and Mahajan, G. 2021. On the Theory of Policy Gradient Methods: Optimality, Approximation, and Distribution Shift. *J. Mach. Learn. Res.*, 22(98): 1–76.
- Akyürek, E.; and Andreas, J. 2022. Compositionality as Lexical Symmetry. [arXiv:2201.12926](https://arxiv.org/abs/2201.12926).
- Alayrac, J.-B.; Donahue, J.; Luc, P.; Miech, A.; Barr, I.; Hasson, Y.; Lenc, K.; Mensch, A.; Millican, K.; Reynolds, M.; et al. 2022. Flamingo: a visual language model for few-shot learning. *arXiv preprint arXiv:2204.14198*.
- Bhambri, S.; Kim, B.; and Choi, J. 2023. Multi-level Compositional Reasoning for Interactive Instruction Following. *Interaction*, 3: 4.
- Bommasani, R.; Hudson, D. A.; Adeli, E.; Altman, R.; Arora, S.; von Arx, S.; Bernstein, M. S.; Bohg, J.; Bosselut, A.; Brunskill, E.; et al. 2021. On the opportunities and risks of foundation models. *arXiv preprint arXiv:2108.07258*.
- Burda, Y.; Edwards, H.; Storkey, A.; and Klimov, O. 2018. Exploration by random network distillation. *arXiv preprint arXiv:1810.12894*.
- Camacho, A.; Icarte, R. T.; Klassen, T. Q.; Valenzano, R. A.; and McIlraith, S. A. 2019. LTL and Beyond: Formal Languages for Reward Function Specification in Reinforcement Learning. In *IJCAI*, volume 19, 6065–6073.
- Ding, D.; Hill, F.; Santoro, A.; Reynolds, M.; and Botvinick, M. 2021. Attention over learned object embeddings enables complex visual reasoning. *Advances in neural information processing systems*, 34: 9112–9124.
- Drexler, D.; Seipp, J.; and Geffner, H. 2021. Expressing and Exploiting the Common Subgoal Structure of Classical Planning Domains Using Sketches: Extended Version. [arXiv:2105.04250](https://arxiv.org/abs/2105.04250).
- Du, Y.; Watkins, O.; Wang, Z.; Colas, C.; Darrell, T.; Abbeel, P.; Gupta, A.; and Andreas, J. 2023. Guiding Pre-training in Reinforcement Learning with Large Language Models. [arXiv:2302.06692](https://arxiv.org/abs/2302.06692).
- Duan, J.; Chen, L.; Tran, S.; Yang, J.; Xu, Y.; Zeng, B.; and Chilimbi, T. 2022. Multi-modal alignment using representation codebook. In *Proceedings of the IEEE/CVF Conference on Computer Vision and Pattern Recognition*, 15651–15660.
- Fei, N.; Lu, Z.; Gao, Y.; Yang, G.; Huo, Y.; Wen, J.; Lu, H.; Song, R.; Gao, X.; Xiang, T.; et al. 2022. Towards artificial general intelligence via a multimodal foundation model. *Nature Communications*, 13(1): 1–13.
- Goyal, P.; Niekum, S.; and Mooney, R. 2021. Pixl2r: Guiding reinforcement learning using natural language by mapping pixels to rewards. In *Conference on Robot Learning*, 485–497. PMLR.
- Goyal, P.; Niekum, S.; and Mooney, R. J. 2019. Using natural language for reward shaping in reinforcement learning. *arXiv preprint arXiv:1903.02020*.
- Hafner, D.; Lillicrap, T.; Norouzi, M.; and Ba, J. 2020. Mastering atari with discrete world models. *arXiv preprint arXiv:2010.02193*.
- Hornik, K.; Stinchcombe, M.; and White, H. 1989. Multilayer feedforward networks are universal approximators. *Neural networks*, 2(5): 359–366.
- Hu, R.; Fried, D.; Rohrbach, A.; Klein, D.; Darrell, T.; and Saenko, K. 2019. Are you looking? grounding to multiple modalities in vision-and-language navigation. *arXiv preprint arXiv:1906.00347*.
- Huang, S.; Papernot, N.; Goodfellow, I.; Duan, Y.; and Abbeel, P. 2017. Adversarial attacks on neural network policies. *arXiv preprint arXiv:1702.02284*.
- Ibarz, B.; Leike, J.; Pohlen, T.; Irving, G.; Legg, S.; and Amodei, D. 2018. Reward learning from human preferences and demonstrations in atari. *Advances in neural information processing systems*, 31.
- Ilahi, I.; Usama, M.; Qadir, J.; Janjua, M. U.; Al-Fuqaha, A.; Hoang, D. T.; and Niyato, D. 2021. Challenges and countermeasures for adversarial attacks on deep reinforcement learning. *IEEE Transactions on Artificial Intelligence*, 3(2): 90–109.
- Janner, M.; Du, Y.; Tenenbaum, J. B.; and Levine, S. 2022. Planning with Diffusion for Flexible Behavior Synthesis. *arXiv preprint arXiv:2205.09991*.
- Kant, Y.; Ramachandran, A.; Yenamandra, S.; Gilitschenski, I.; Batra, D.; Szot, A.; and Agrawal, H. 2022. Housekeep: Tidying Virtual Households using Commonsense Reasoning. [arXiv:2205.10712](https://arxiv.org/abs/2205.10712).
- Kaplan, R.; Sauer, C.; and Sosa, A. 2017. Beating atari with natural language guided reinforcement learning. *arXiv preprint arXiv:1704.05539*.
- Li, J.; Li, D.; Savarese, S.; and Hoi, S. 2023. BLIP-2: Bootstrapping Language-Image Pre-training with Frozen Image Encoders and Large Language Models. [arXiv:2301.12597](https://arxiv.org/abs/2301.12597).
- Lin, J.; Fried, D.; Klein, D.; and Dragan, A. 2022. Inferring rewards from language in context. *arXiv preprint arXiv:2204.02515*.
- Liu, X.; Palacios, H.; and Muise, C. 2022. A planning based neural-symbolic approach for embodied instruction following. *Interactions*, 9(8): 17.
- Luketina, J.; Nardelli, N.; Farquhar, G.; Foerster, J.; Andreas, J.; Grefenstette, E.; Whiteson, S.; and Rocktäschel, T. 2019. A survey of reinforcement learning informed by natural language. *arXiv preprint arXiv:1906.03926*.
- Mitkov, R. 2014. *Anaphora resolution*. Routledge.
- Ng, A. Y.; Harada, D.; and Russell, S. 1999. Policy invariance under reward transformations: Theory and application to reward shaping. In *ICML*, volume 99, 278–287.
- Okudo, T.; and Yamada, S. 2021. Subgoal-based reward shaping to improve efficiency in reinforcement learning. *IEEE Access*, 9: 97557–97568.
- Ouyang, L.; Wu, J.; Jiang, X.; Almeida, D.; Wainwright, C. L.; Mishkin, P.; Zhang, C.; Agarwal, S.; Slama, K.; Ray, A.; et al. 2022. Training language models to follow instructions with human feedback. *arXiv preprint arXiv:2203.02155*.

- Pham, T. M.; Bui, T.; Mai, L.; and Nguyen, A. 2020. Out of Order: How important is the sequential order of words in a sentence in Natural Language Understanding tasks? *arXiv preprint arXiv:2012.15180*.
- Raffel, C.; Shazeer, N.; Roberts, A.; Lee, K.; Narang, S.; Matena, M.; Zhou, Y.; Li, W.; and Liu, P. J. 2020. Exploring the Limits of Transfer Learning with a Unified Text-to-Text Transformer. *arXiv:1910.10683*.
- Sarkar, A.; Feng, J.; Vorobeychik, Y.; Gill, C.; and Zhang, N. 2022. Reward delay attacks on deep reinforcement learning. *arXiv preprint arXiv:2209.03540*.
- Schulman, J.; Wolski, F.; Dhariwal, P.; Radford, A.; and Klimov, O. 2017. Proximal policy optimization algorithms. *arXiv preprint arXiv:1707.06347*.
- Seo, Y.; Hafner, D.; Liu, H.; Liu, F.; James, S.; Lee, K.; and Abbeel, P. 2022. Masked world models for visual control. *arXiv preprint arXiv:2206.14244*.
- Talvitie, E.; and Bowling, M. H. 2015. Pairwise Relative Offset Features for Atari 2600 Games. In *AAAI Workshop: Learning for General Competency in Video Games*. Citeseer.
- Vaswani, A.; Shazeer, N.; Parmar, N.; Uszkoreit, J.; Jones, L.; Gomez, A. N.; Kaiser, Ł.; and Polosukhin, I. 2017. Attention is all you need. *Advances in neural information processing systems*, 30.
- Wang, C.-Y.; Bochkovskiy, A.; and Liao, H.-Y. M. 2022. YOLOv7: Trainable bag-of-freebies sets new state-of-the-art for real-time object detectors. *arXiv:2207.02696*.
- Wang, L.; Javed, Z.; Wu, X.; Guo, W.; Xing, X.; and Song, D. 2021. Backdoor!: Backdoor attack against competitive reinforcement learning. *arXiv preprint arXiv:2105.00579*.
- Wang, X.; Huang, Q.; Celikyilmaz, A.; Gao, J.; Shen, D.; Wang, Y.-F.; Wang, W. Y.; and Zhang, L. 2019. Reinforced cross-modal matching and self-supervised imitation learning for vision-language navigation. In *Proceedings of the IEEE/CVF Conference on Computer Vision and Pattern Recognition*, 6629–6638.
- Wiewiora, E.; Cottrell, G. W.; and Elkan, C. 2003. Principled methods for advising reinforcement learning agents. In *Proceedings of the 20th international conference on machine learning (ICML-03)*, 792–799.
- Xiao, L. 2022. On the convergence rates of policy gradient methods. *arXiv preprint arXiv:2201.07443*.
- Xu, H.; Ye, Q.; Yan, M.; Shi, Y.; Ye, J.; Xu, Y.; Li, C.; Bi, B.; Qian, Q.; Wang, W.; Xu, G.; Zhang, J.; Huang, S.; Huang, F.; and Zhou, J. 2023. mPLUG-2: A Modularized Multimodal Foundation Model Across Text, Image and Video. *arXiv:2302.00402*.
- Xuan, H.; Stylianou, A.; Liu, X.; and Pless, R. 2020. Hard negative examples are hard, but useful. In *European Conference on Computer Vision*, 126–142. Springer.
- Yang, T.-Y.; Hu, M. Y.; Chow, Y.; Ramadge, P. J.; and Narasimhan, K. 2021. Safe reinforcement learning with natural language constraints. *Advances in Neural Information Processing Systems*, 34: 13794–13808.
- Zhang, X.; Chen, Y.; Zhu, X.; and Sun, W. 2021. Robust policy gradient against strong data corruption. In *International Conference on Machine Learning*, 12391–12401. PMLR.
- Zhang, X.; Ma, Y.; Singla, A.; and Zhu, X. 2020. Adaptive reward-poisoning attacks against reinforcement learning. In *International Conference on Machine Learning*, 11225–11234. PMLR.

A Implementation Details

Computation The experiments were tested on a single NVIDIA GeForce RTX 3090 GPU, with 8 CPU cores. Each training trial is run for a total of 20 million frames. Average duration for each trial is around 1 hour.

Environment hyperparameter

Table 4: Hyperparameter of the Montezuma’s Revenge game environment

Hyperparameter	Value
Grey-scaling	True
Observation Resize	(84,84)
Language reward clipping	[0,1]
Intrinsic reward clipping	[0,5]
Environmental reward clipping	[0,1]
Max frames per episode	1200
Terminal on loss of life	False
Max and skip frames	4
Random starts	30
Sticky action probability	0.25
Frames stacked	4
Size of action space	8
image normalization mean	[0.485 * 255.0, 0.456 * 255.0, 0.406 * 255.0]
image normalization std	[0.229 * 255.0, 0.224 * 255.0, 0.225 * 255.0]
random seed	{1,2,3,4,5,6,7,8,9,10}

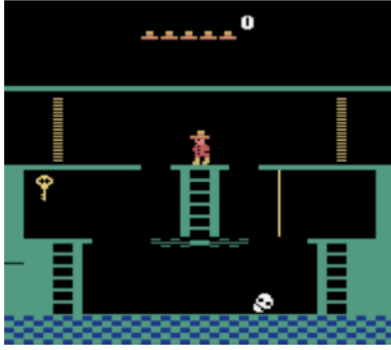
Model hyperparameter

Table 5: Hyperparameter of the PPO+RND policy model

Hyperparameter	Value
learning rate	1.0e-4
Rollout length	128
env gamma	0.99
language gamma	0.99
intrinsic gamma	0.99
use GAE	True
GAE lambda	0.95
mini batch	4
Entropy coefficient	0.001
env and lang reward coefficient	3.0
intrinsic reward coefficient	1.0
Size of action space	8
Policy architecture	CNN
batch size	256
number of parallel environments	8

The task environment Room A2 and the associated natural language instructions

Task environment

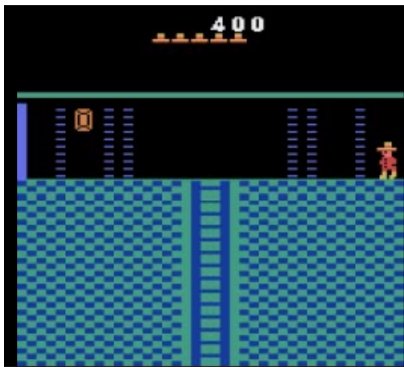


Instructions of the task

1. Go down that ladder and walk right on the conveyor belt.
2. Jump to the yellow rope and again jump to the platform on the right
3. Go down the ladder here and wait for the skull to approach and jump over it
4. Go up the ladder at the left end, jump to grab the key
5. Back to where you started, walk through the door on the left.

The task environment Room A1 and the associated natural language instructions

Task environment



Instructions of the task

1. The next room will introduce a laser gates. Avoid running right away or you might run right into the first laser gate. Instead, inch toward to the first one and wait for it to shut off and then run past it.
2. Don't try to run past the next set of laser gates because you won't make it.
3. Just be patient and make your way to the gem at the far left.

The task environment Room B3 and the associated natural language instructions

Task environment



Instructions of the task

1. Walk through the door on your right and then jump onto the purple rope.
2. Climb up a bit and wait for the skull to roll to the left and then jump off.
3. Jump over the skull when it comes back to the right.
4. Make a final jump to the white rope off the left side of the platform and climb up.
5. Jump right and then grab the torch hanging above the conveyor belt.

Evaluation Metrics We set a cap on the number of wins an agent can achieve during training at 1500. This means that once the agent reaches this limit, the training process will automatically stop. We assume that the training becomes stable after reaching this limit. The evaluation metric is the area under the curve (AUC) normalised by the length of training episodes. Specifically, we calculate the AUC by summing up the number of wins achieved at each time step i during training and dividing it by the total number of training episodes T . It can be expressed as:

$$AUC = \frac{\sum_{i=0}^T \text{no. of win}_i}{T}$$

B Implementation details for Simulated LRS models

For each environment tested, we first defined sets of target trajectories $\tau_i^{\Pi_G}$ that correspond to each instruction sentence D_i . During policy training, the simulated LRS model receives the current trajectory of the agent $\tau^\pi = \{s_0, a_0, s_1, \dots, a_{t-1}, s_t\}$ at each time t . It then compares τ^π with the sets of predefined target trajectories $\{\tau_i^{\Pi_G}\}$ and provides immediate rewards according to reward rules stated in Table 1.

Rule 1 simulates a type of LRS model that does not reward partially matched trajectories. Rule 2 and Rule 3 simulates LRS models that reward partially matched trajectories. The difference between the two is that in Rule 2, the temporal ordering constraints are strictly maintained by heuristics, while in Rule 3, partially matched trajectories that do not satisfy temporal constraints can also be rewarded. To simplify our analysis, we focus solely on one type of temporal constraint, which is the order in which each instruction sentence is executed. Therefore, temporal constraints are met if the agent’s trajectory matches the correct order of the target trajectory sequence. For example, if τ^π matches with $\tau_i^{\Pi_G} + \tau_{i+1}^{\Pi_G}$, we say τ^π fulfils the temporal constraints.

It is important to note that the reward rule in Table 1 ensures that the rollout cumulative rewards of partially matched trajectories will always be smaller than that of fully matched ones. This ensures that the RL algorithm will converge eventually in theory.

C Detailed Experiment Result Tables

In this study, we focus on the PPO+RND RL backbone, given that LRS methods are typically harnessed for tasks with sparse reward signals, a scenario where the PPO algorithm alone has been proven ineffective (Schulman et al. 2017; Burda et al. 2018). The vanilla “PPO+RND” model serves as the baseline, and we compare it with ones supplemented by various LRS models. The inclusion of “PPO + Sim LRS Rule 1” in Table 6 is merely to illustrate that under ideal conditions, LRS is intended to support PPO in overcoming its ineffectiveness with sparse reward tasks. By showing that the PPO+RND model can be significantly hindered by issue of rewarding partially matched trajectories, we demonstrate the brittleness of the existing LRS techniques. The PPO algorithm will only magnify this issue, given its comparative ineffectiveness against RND when faced with sparse-reward settings.

Table 6: Learning efficiency of agents in Room A2 of Montezuma’s Revenge game, measured by AUC (higher is better), and success rate (for perturbed rewards tolerance). Baseline denoted as B. \star indicates statistical significance ($p < 0.05$).

Model	AUC (higher is better)	p-value w.r.t. B	success rate
PPO (Schulman et al. 2017)	all failed	-	0%
PPO+RND (B)	0.633±0.038	-	100%
PPO + Sim LRS Rule 1	0.287±0.048	4.5e-05 \star	100%
PPO+RND + Non-Sim LRS	all failed	\star	0%
PPO+RND + Sim LRS Rule 1	0.571±0.028	8.5e-04 \star	100%
PPO+RND + Sim LRS Rule 2	0.165±0.206	4.3e-06 \star	70%
PPO+RND + Sim LRS Rule 3	all failed	\star	0%

Table 7: Learning efficiency of agents in Room A1 of Montezuma’s Revenge game, measured by AUC (higher is better), and success rate (for perturbed rewards tolerance). Baseline denoted as B. \star indicates statistical significance ($p < 0.05$).

Model	AUC (higher is better)	p-value w.r.t. B	success rate
PPO	all failed	-	0%
PPO+RND (B)	0.201±0.038	-	100%
PPO+RND + Non-Sim LRS	0.174±0.220	0.32	40%
PPO+RND + Sim LRS Rule 1	0.433±0.085	0.99	100%
PPO+RND + Sim LRS Rule 2	0.225±0.229	0.61	50%
PPO+RND + Sim LRS Rule 3	0.152±0.201	0.14	50%

Table 8: Learning efficiency of agents in Room B3 of Montezuma’s Revenge game, measured by AUC (higher is better), and success rate (for perturbed rewards tolerance). Baseline denoted as B. \star indicates statistical significance ($p < 0.05$).

Model	AUC (higher is better)	p-value w.r.t. B	success rate
PPO	all failed	-	0%
PPO+RND (B)	0.817±0.101	-	100%
PPO+RND + Non-Sim LRS	0.033±0.099	1.1e-12 \star	10%
PPO+RND + Sim LRS Rule 1	0.821±0.090	0.53	100%
PPO+RND + Sim LRS Rule 2	0.161±0.103	3.5e-11 \star	100%
PPO+RND + Sim LRS Rule 3	all failed	\star	0%

D Proofs

D.1 Proof of convergence guarantee of the potential-based perfect LRS (Proposition 3.5)

The proof is derived firmly anchored in the foundational work present in Wiewiora, Cottrell, and Elkan (2003) and Okudo and Yamada (2021). The convergence guarantee property is only applicable to on-policy RL algorithms such as SARSA and PPO. We start by proving $F(s_t, a_t, s_{t-1}, a_{t-1}) = \Phi(s_t, a_t) - \gamma^{-1}\Phi(s_{t-1}, a_{t-1})$ is a potential-based reward shaping function (i.e., the optimal policy in the old setting remains optimal when the reward function is modified by adding the reward shaping function). We first of all write down the optimal Q-value of the original MDP:

$$Q^*(s, a) = \mathbb{E}\left[\sum_{t=0}^{\infty} \gamma^t R_t^{\text{env}} \mid s_0 = s, \pi = \pi^*\right] \quad (1)$$

We now write down the optimal Q-value when the reward function is modified with the shaping reward, we denote it as Q_{Φ}^* :

$$\begin{aligned} Q_{\Phi}^*(s, a) &= \mathbb{E}\left[\sum_{t=0}^{\infty} \gamma^t (R_t^{\text{env}} + F_t)\right] \\ &= \mathbb{E}\left[\sum_{t=0}^{\infty} \gamma^t (R_t^{\text{env}} + \Phi(s_t, a_t) - \gamma^{-1}\Phi(s_{t-1}, a_{t-1}))\right] \\ &= \mathbb{E}\left[\sum_{t=0}^{\infty} \gamma^t R_t^{\text{env}}\right] + \mathbb{E}\left[\sum_{t=0}^{\infty} \gamma^t \Phi(s_t, a_t)\right] - \mathbb{E}\left[\sum_{t=-1}^{\infty} \gamma^t \Phi(s_t, a_t)\right] \\ &= \mathbb{E}\left[\sum_{t=0}^{\infty} \gamma^t R_t^{\text{env}}\right] - \gamma^{-1}\mathbb{E}[\Phi(s_{-1}, a_{-1})] \\ &= Q^*(s, a) - \gamma^{-1}\mathbb{E}[\Phi(s_{-1}, a_{-1})] \end{aligned} \quad (2)$$

The term $\mathbb{E}[\Phi(s_{-1}, a_{-1})]$ refers to the expected value of the potential function Φ of the previous state and action, given π . They are considered as the exploration history and will not impact the current update when RL algorithms are on-policy. Thus the optimal policy remains. Since instruction guides the learning agent to reach the final goal, it can be seen as telling the agent what subgoals are required in order to reach the final goal. the potential function can be set as $\Phi(s_t, a_t) = \alpha \times c(s_t, a_t)$, where α is a hyperparameter and $c(s_t, a_t)$ is a function that outputs the sequence number of the subgoal that the (s_t, a_t) tuple contributes to. Therefore, the final shaping reward function F can be seen as measuring the increment of the achieved subgoals from the last state. Thus, we proved that LRS function is approximately a potential-based shaping function and the optimal policy invariance is guaranteed.

Clarification: It’s crucial to recognize that while the “look-back” potential-based shaping function may appear non-Markovian – given its reliance on preceding states and actions – its true essence lies in a specific constraint: the shaping reward is tailored exclusively for on-policy RL algorithms such as PPO and RND. This distinction ensures that the term $\mathbb{E}[\Phi(s_{-1}, a_{-1})]$ is interpreted solely as a record of exploration history, without influencing the contemporaneous update of the on-policy model.

The reason why the “look-ahead” reward function $F(s, a, s', a') = \gamma\Phi(s', a') - \Phi(s, a)$ is not applicable here is because it imposes a strong assumption requiring the potential function to remain deterministic and stable in order to have the optimal policy unchanged. However, this condition is not satisfied for LRS because the reward function undergoes updates in each iteration. Wiewiora, Cottrell, and Elkan (2003) provides a comprehensive explanation regarding this matter.

D.2 Proof of the Reduction of Convergence Rate

Specifically, the update rule of Actor-Critic algorithm is:

- **Critic:**

$$\phi \leftarrow \phi - \alpha_\phi \nabla_\phi (\delta)^2 \quad (3)$$

where

$\delta = \mathbb{E}_{\pi_\theta} [G^{\pi_\theta} - Q_\phi(s, a)]$ is the Monte Carlo (MC) estimation error,
 G^{π_θ} is the rollout cumulative rewards from the trajectory τ^{π_θ} generated from π_θ .

- **Actor:**

$$\theta \leftarrow \theta + \alpha_\theta \frac{Q_\phi(s, a) \nabla_\theta \pi_\theta(a|s)}{\pi_\theta(a|s)} \quad (4)$$

We need to make the following assumptions to simplify the theoretical analysis:

1. We use Π_G to represent the set of acceptable policies and use Π_L as an arbitrary set of suboptimal policies that are partially consistent with the instruction. For simplicity, we also assume $\Pi_L \cap \Pi_G = \emptyset$, meaning that Π_L cannot reach the goal state.
2. Assume the policy class parameterized by θ should be expressive enough to capture optimal or near-optimal policies, and the policy is initialised randomly from uniform distribution, i.e., $\pi_{\theta_0} \sim \mathcal{U}(\Pi)$. Meanwhile, $Q_{\phi_0}(s, a) = 0, \forall s \in \mathcal{S} \forall a \in \mathcal{A}$, where Q -value function measured the expected discounted cumulative reward given the state s and action a .
3. We assume that $|\Pi_G|$ and $|\Pi_L|$ is a fixed number predefined by the task environment while $\mathbb{E}[G^\pi | \pi \in \Pi_L]$ is non-zero as partially matched trajectories are rewarded.

Since the update rule for Q -value is a gradient descent on $\|\mathbb{E}[G^{\pi_\theta} - Q_\phi(s, a)]\|^2$ and also we have that $\{\Pi_L, \Pi_G, \Pi \setminus (\Pi_L \cup \Pi_G)\}$ is a countable partition of the policy universe Π , the updated Q -value will approach as follows:

$$\begin{aligned} Q_\phi(s, a) &\rightarrow \mathbb{E}[G^{\pi_\theta}] \\ &= P(\pi_\theta \in \Pi_L) \cdot \mathbb{E}[G^{\pi_\theta} | \pi_\theta \in \Pi_L] + P(\pi_\theta \in \Pi_G) \cdot \mathbb{E}[G^{\pi_\theta} | \pi_\theta \in \Pi_G] \\ &\quad + P(\pi_\theta \in \Pi \setminus (\Pi_L \cup \Pi_G)) \cdot \mathbb{E}[G^{\pi_\theta} | \pi_\theta \in \Pi \setminus (\Pi_L \cup \Pi_G)] \\ &= P(\pi_\theta \in \Pi_L) \cdot \mathbb{E}[G^{\pi_\theta} | \pi_\theta \in \Pi_L] + P(\pi_\theta \in \Pi_G) \cdot \mathbb{E}[G^{\pi_\theta} | \pi_\theta \in \Pi_G] \end{aligned} \quad (5)$$

Given that the update rule for policy π is the gradient ascent on $Q_\phi(s, a) \pi_\theta(a|s)$, we have the following:

$$\begin{aligned} &\nabla_\theta Q_\phi(s, a) \pi_\theta(a|s) \\ &= (\nabla_\theta P(\pi_{\theta_{old}} \in \Pi_L) \cdot \mathbb{E}[G^{\pi_{\theta_{old}}} | \pi_{\theta_{old}} \in \Pi_L] \pi_\theta(a|s)) \\ &\quad + (\nabla_\theta P(\pi_{\theta_{old}} \in \Pi_G) \cdot \mathbb{E}[G^{\pi_{\theta_{old}}} | \pi_{\theta_{old}} \in \Pi_G] \pi_\theta(a|s)) \\ &= P(\pi_L) \cdot \mathbb{E}[G^{\pi_L}] \nabla_\theta \pi_\theta(a|s) + P(\pi_G) \cdot \mathbb{E}[G^{\pi_G}] \nabla_\theta \pi_\theta(a|s) \\ &= (1 - P(\pi_G) - P(\pi_\theta \in \Pi \setminus (\Pi_L \cup \Pi_G))) \cdot \mathbb{E}[G^{\pi_L}] \nabla_\theta \pi_\theta(a|s) + P(\pi_G) \cdot \mathbb{E}[G^{\pi_G}] \nabla_\theta \pi_\theta(a|s) \\ &= const \cdot \mathbb{E}[G^{\pi_L}] \nabla_\theta \pi_\theta(a|s) + (\mathbb{E}[G^{\pi_G}] - \mathbb{E}[G^{\pi_L}]) P(\pi_G) \nabla_\theta \pi_\theta(a|s) \end{aligned} \quad (6)$$

Justification of the assumptions:

- Regarding the non-zero probability of recovering the optimal policy at initialization, it is standard in theoretical analyses to assume a uniform distribution of a random variable at initialization (see (Agarwal et al. 2021)). This assumption does not contradict the conclusion about the convergence rate deterioration in Theorem 4.1.
- In reference to the realizability condition implied by Assumption 2, the expressiveness of the policy class parameterized by θ is an underlying assumption for deep learning models, supported by the The Universal Approximation Theorem (Hornik, Stinchcombe, and White 1989).

E Temporal constraints from language instructions and Linear Temporal Logic

As a start, we give the definition of atomic sentence – in logic, an atomic sentence is a declarative sentence cannot be further broken down into other simpler sentences. For example, “go down that ladder” is an atomic sentence; “walk right on the conveyor belt” is also an atomic sentence, whereas “go down that ladder and walk right on the conveyor belt” is a molecular sentence in natural language. However, an atomic sentence in natural language usually does not correspond to a single (s, a, s') state-action-next-state transition tuple. For instance, the atomic sentence “go down that ladder” may corresponds to a longer state-action sequence $(s_{\text{AtLadderTop}}, a_{\text{down}}, s_{\text{AtLadderMiddle}}, a_{\text{down}}, s_{\text{AtLadderBottom}})$ because the ladder is long enough that it requires an agent to perform two steps of the “down” actions. Hence, for simplicity, we call the corresponding state-action sequence of an atomic sentence “an atomic event”, labeled as e . Therefore, an agent trajectory τ can be written as a sequence of atomic events, i.e., $\tau = (e_0, e_1, e_2, \dots)$, where e_t is the atomic event at t^{th} order.

The example of modular instruction sentence “go down that ladder and walk right on the conveyor belt” reflects a preference towards a set of trajectory that can be expressed as (e_a, \dots, e_b) , where e_a is the event of going down the ladder and e_b is the event of walking right on the conveyor belt, and there can be arbitrary number of unmentioned atomic events in between. However, if the sentence becomes “go down that ladder after walking right on the conveyor belt”, the preferred trajectories becomes (e_b, \dots, e_a) .

The replacement from the word “and” to the word “after” leads to change of the trajectory preference. In natural language, such a word indicates the temporal relation between the two mentioned atomic sentences. In order to avoid ambiguity, Linear Temporal Logic (LTL), a formal language, will be used to translate the natural language instructions because it can provide a mathematically precise notation for expressing the temporal relations between those atomic sentences.

Specifically, LTL is the extension of propositional logic with two extra temporal modal operators: \bigcirc (next) and \mathbf{U} (until). Given a set of the propositional atomic sentence symbols P , the syntax of an LTL formula is defined according to the following grammar:

$$\phi ::= \text{true} \mid p \mid \phi_1 \wedge \phi_2 \mid \neg\phi \mid \bigcirc\phi \mid \phi_1 \mathbf{U} \phi_2 \quad , \text{ where } p \in P \quad (7)$$

The \mathbf{U} operator can further derive two more temporal modal operators \diamond (eventually, i.e., sometimes in the future) and \square (always, i.e., from now on forever):

$$\begin{aligned} \diamond\phi &:= \text{true} \mathbf{U} \phi \\ \square\phi &:= \neg \diamond \neg\phi \end{aligned} \quad (8)$$

An LTL formula can be satisfied by an infinite trajectory sequence of truth assignment of atomic event variables, i.e., $\tau = (e_0, e_1, e_2, \dots)$ for E , where $p \in e_i$ iff the propositional atomic sentence $p \in P$ holds at time step i . Formally, the satisfaction relation between a trajectory τ at time i and an LTL formula ϕ , denoted by $\langle \tau, i \rangle \models \phi$, is defined as follows:

$$\begin{aligned} \langle \tau, i \rangle &\models \text{true} \\ \langle \tau, i \rangle &\models p \quad \text{iff} \quad p \in e_i \quad (\text{i.e., } e_i \models p) \\ \langle \tau, i \rangle &\models \phi_1 \wedge \phi_2 \quad \text{iff} \quad \langle \tau, i \rangle \models \phi_1 \quad \text{and} \quad \langle \tau, i \rangle \models \phi_2 \\ \langle \tau, i \rangle &\models \neg\phi \quad \text{iff} \quad \langle \tau, i \rangle \not\models \phi \\ \langle \tau, i \rangle &\models \bigcirc\phi \quad \text{iff} \quad \langle \tau, i+1 \rangle \models \phi \\ \langle \tau, i \rangle &\models \phi_1 \mathbf{U} \phi_2 \quad \text{iff} \quad \exists j, i \leq j \quad \text{and} \quad \langle \tau, j \rangle \models \phi_2, \quad \text{and} \quad \langle \tau, k \rangle \models \phi_1 \quad \text{for all } k \in [i, j) \end{aligned} \quad (9)$$

We give a sketch for the semantics of temporal modalities to better understand it.

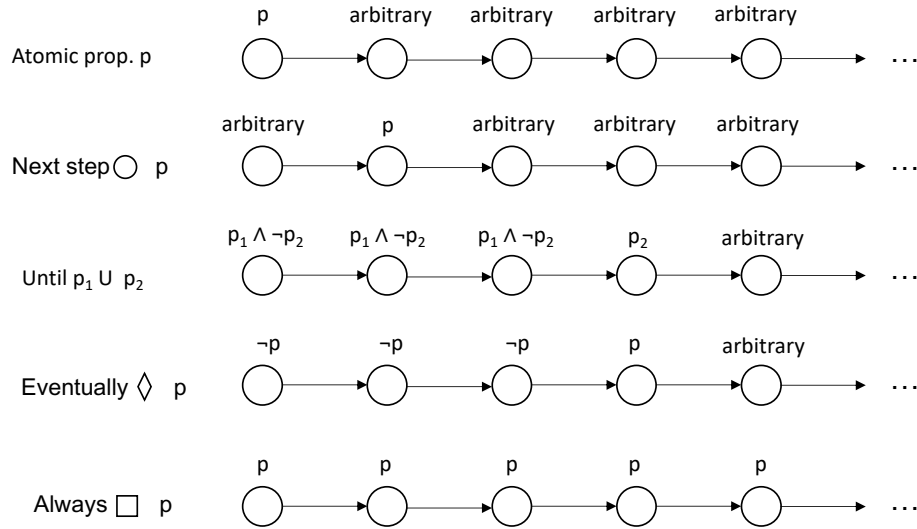


Figure 7: Sketch of semantics of temporal modalities

Now we go back to the example “go down that ladder and walk right on the conveyor belt but do not fall off the conveyor belt”. It can be expressed in LTL as $\diamond(p_1 \wedge p_2) \wedge \square \neg p_3$, where p_1, p_2, p_3 are the propositions that are true if and only if the corresponding atomic events “go down that ladder”, “walk right on the conveyor belt”, “fall off the conveyor belt” are performed. And we say an agent trajectory is consistent with the temporal constraints of the language instruction iff the trajectory satisfies

the LTL formula of the instruction. Note that the LTL formulae address only the temporal relationship between events, but not deal with the recognition of events.

LTL supports non-Markovian constraints, though the setting of the task environment in this work is Markovian. However, we will not go into details of that.

F Raw Results Plots

We list all the raw result plots with the format shown in Table 9:

Table 9: Structure of the raw result plots

cumulative rewards for the first instruction sentence	cumulative rewards for the second instruction sentence	cumulative rewards for the third instruction sentence	cumulative rewards for the fourth instruction sentence	cumulative rewards for the fifth instruction sentence
Number of cumulative achieved state constraints	Number of cumulative achieved action constraints	Number of win over training samples	Global training steps	gaming steps (i.e., duration) per training episode
Environmental Rewards per training episode	Number of policy model update	Number of sample episodes	intrinsic reward per global update (RND algorithm)	max probability of an action per global update (measures the confidence level of the policy)

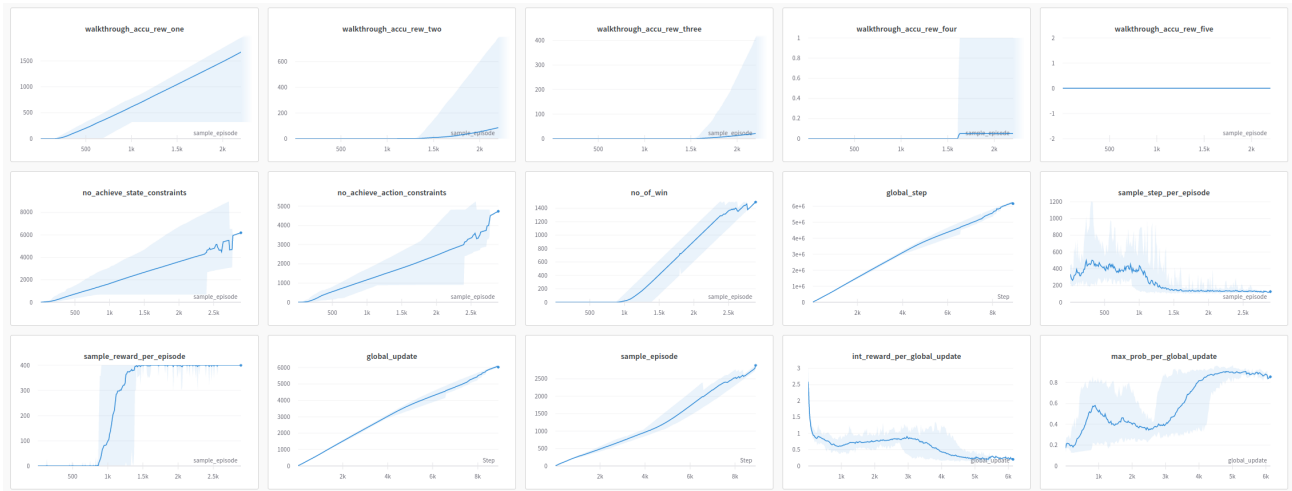


Figure 8: LRS Model A raw results plot



Figure 9: LRS Model B raw results plot



Figure 10: LRS Model C raw results plot



Figure 11: LRS Model A with Low Granularity Type 1 raw results plot



Figure 12: LRS Model A with Low Granularity Type 2 raw results plot



Figure 13: Vanilla PPO+RND raw results plot

G Implementation Details of Non-Simulated LRS Binary Classifier

Originally this work was targeting to improve the precision score of LRS binary classifier. Although this paper proved that such a mechanism leads to performance deterioration of the instruction following agent, we would like still list some of the techniques we found useful for improving model’s precision. Notice that some methods may be specific to Montezuma’s Revenge game environment.

G.1 Pretraining a visual autoencoder to compress visual observations into dense feature vectors

Pretraining a visual encoder such that pixel-based visual observations (e.g., $T \times 3 \times 84 \times 84$ rgb video clip of length T) can be compressed into dense features vectors that capture spatial and temporal information. It helps to reduce the input dimension and thereby speeding up the learning process. Many recent work on RL used such a pretraining method (Hafner et al. 2020; Seo et al. 2022).

G.2 Soft-discretisation of visual inputs

With the help of an object detector, the visual perception module of the instruction-following agent can to some extent discretizes the pixel-based visual information to a object-based one (see Figure 14). Given that reasoning process only applies to atomic evidence, and also that physical reasoning in most instruction-following tasks is conducted at the object level, it is argued that the “discretisation” process helps to improve the overall performance of the reasoning model. This method has been discussed in recent studies. Hu et al. (2019) suggested that object presentation increased the success rate for Visual Language Navigation tasks. Ding et al. (2021) also mentioned the performance improvement on Visual Question Answering (VQA) tasks by converting the pixel images into object-based representations first.

G.3 Relative offsets to capture the spatial relationships

Instead of using the original visual observation obs_t as input at time t , one can use the relative offset $obs_t - obs_{t-1}$ in order to emphasise the spatial relationship between objects. This approach is also known as B-PRO from Talvitie and Bowling (2015), which has been shown effective in shortening the required training steps. This approach is effective especially for Montezuma’s Revenge game because the relative offset operation can effectively cancel out the unimportant background information. It remains unclear that this approach is still useful when the environment background becomes dynamic and noisy.

G.4 Phrase corruption technique, a clever way to generate hard negative training samples

Training with hard negative samples helps to reduce the false positive errors (Xuan et al. 2020). However, the trajectory-instruction data pairs for training are all positive pairs and most common techniques such as in-batch negative sampling are not able to generate hard-negatives. Language instructions are made up of object and action constraints. In light of this, we propose the “phrase corruption” technique – it will “corrupt” the object and action constraints by only replacing the action and the object phrases in the language sentences. We consider the new generated instructions as hard negative samples because only the semantic of the instructions are changed while the original sentence structures and the tones are largely maintained. The procedure is as follows – first, we use a off-the-shelf phrase chunking model to chunk the instruction into phrases, meanwhile we extract all the verb and noun phrases from the dataset into two separate phrase set. After that, for each instruction sentence, we randomly select one phrase from the phrase set to replace the original noun and verb phrases (see Figure 15). Although this

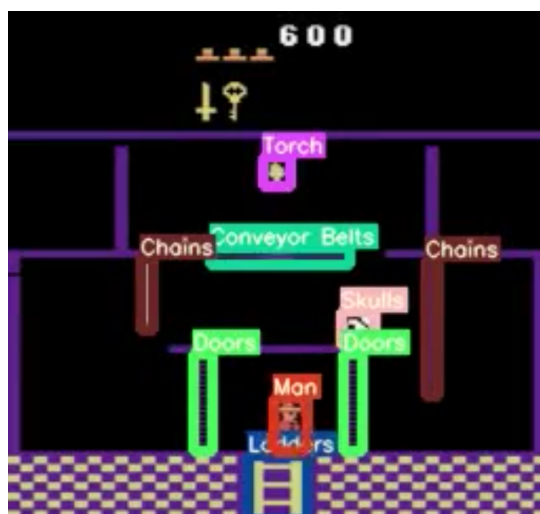


Figure 14: An example of having an object detector to annotate the visual input

method can help to generate a large number of hard-negative texts, some samples may not logically make sense (e.g., climb down the ladder → ~~climb down~~ kill the ladder).

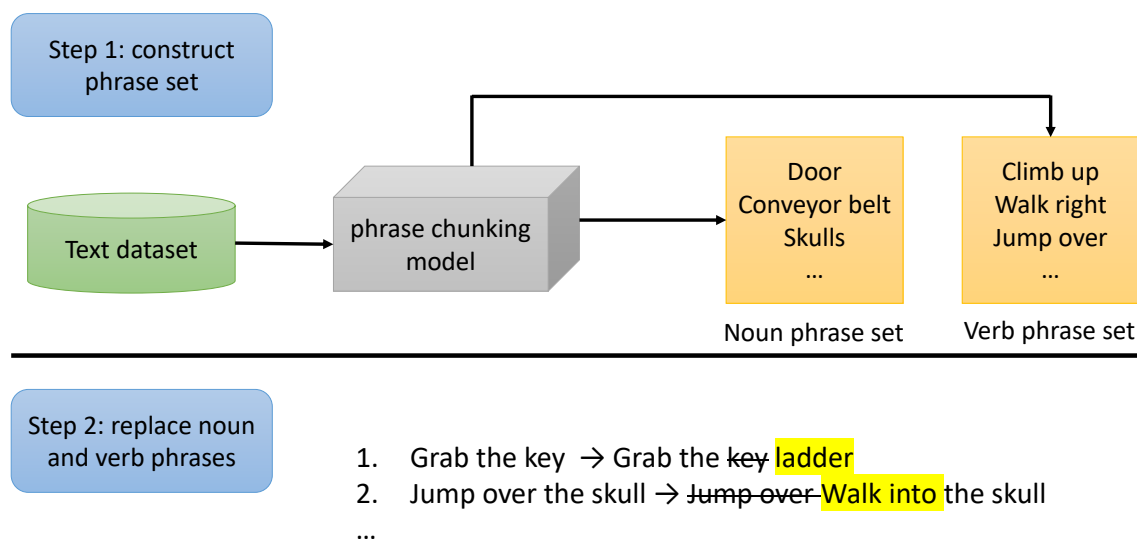


Figure 15: An illustration of the “phrase corruption” procedure

G.5 Implementation details during policy training

In the policy training process, we manually partition the language instructions into atomic sentences. For each policy update iteration, the agent’s past trajectory is converted into embedding vectors and fuse together with the currently focused atomic sentence. We assume the agent has fulfilled the current instruction when the matching score exceeds a manually defined threshold, causing the activation of the next atomic sentence.

G.6 Overall results on different ablation settings

We trained a LRS binary classifier on an annotated trajectory dataset from Goyal, Niekum, and Mooney (2019). It consists of 5000 annotated human player replay clips with 3 second each. Annotations are obtained by using Amazon Mechanical Turk and are made up of one single sentence about what is happening in the 3-second demonstration ². The testing dataset is made

²The annotation dataset can be downloaded from <http://www.cs.utexas.edu/~pgoyal/atari-lang.zip>

by ourselves which follows the same patterns as the Goyal et al.'s. The performance of the LRS binary classifier with different ablation settings is shown in Table 10.

Table 10: Evaluation of the metrics on different ablation settings for LRS binary classifier

Ablation Settings				Precision	Recall	Bal Acc
Pretraining	Discretisation	Relative-Offset	Phrase Corruption			
X	X			40.00%	40.00%	55.00%
X	X	X		50.00	40.00%	60.00%
X	X	X	X	66.67%	80.00%	70.00%